Photochemical & Photobiological Sciences

PAPER

View Article Online
View Journal | View Issue

Cite this: *Photochem. Photobiol. Sci.*, 2016, **15**, 1544

Monomolecular pyrenol-derivatives as multi-emissive probes for orthogonal reactivities†‡

Björn Finkler,[a] Iris Riemann,[b] Michael Vester,[a] Andreas Grüter,[a] Frank Stracke[b] and Gregor Jung*[a]

Received 8th August 2016,
Accepted 27th October 2016

DOI: 10.1039/c6pp00290k

www.rsc.org/pps

Photoacids on the basis of pyrenol have been extensively studied in the past 60 years. As their photophysical properties strongly depend on the substituents at the aromatic scaffold, we introduced two reactive moieties with different electronic coefficients thus creating multi-wavelength fluorescent probes. One probe is capable of monitoring two orthogonal transformations by four fluorescence colors, distinguishable even by the naked human eye. Another derivative can act as a three-color sensor for a wide range of different pH values. Both the presented compounds allow for mimicking of fundamental and advanced two-input logic operations due to the multi-wavelength emission. Furthermore, these compounds can process information in a logically reversible way (Feynman gate).

Introduction

Information processing with optical probes enables rapid and sensitive detection of different analytes in biochemical and supramolecular systems.[1–3] Fluorogenic substrates, which represent a logic YES-gate, are widely used for the detection and activity determination of enzymes due to the high sensitivity of fluorescence based methods.[1,4–9] Yet, measurements with on–off probes impose complications in quantification,[10,11] which are largely overcome by the use of dual-emissive probes, *i.e.* a YES and a NOT gate in a single molecule.[2,3,11–16] Enzymes with their fundamental importance for the function of biological systems are one of the key objectives of these probes. Since multianalyte systems are promising tools for "smart" medical diagnostics,[17–20] probes for multiple enzymes are of particular interest. So far, only a few single probes for two enzymes have been reported.[17,21–23] Most of these examples are fluorogenic since they emit only fluorescence if both enzymes are present and can monitor only a combined activity of both enzymes. When only one or the other enzyme is present, these systems provide no information. A separate single enzyme probe would be necessary to address this scenario. One notable exception that enables resolution of individual enzyme activity with a cleavable FRET-pair is presented by Li *et al.*[21] While the fluorogenic probes can be seen as AND gates, this latter example "has to be regarded as an OR logic gate",[22] since a clear assignment of the corresponding metabolization states to the emission spectra is demanding for this probe. Here we present the ratiometric, monomolecular dual enzyme probe **1**. The probe utilizes the spectral differences of a photoacid and the corresponding base as well as the sensitivity of the pyrene based photoacids to modifications which alter the electron-withdrawing strength of the aromatic substituents. Our system exhibits four distinct metabolization states denoted by four easily distinguishable fluorescence colors. Since phosphatase activity is an important marker for several human diseases[13,24,25] and carboxyl esterase plays a key role in detoxification processes and drug targeting,[12,16,26] these enzymes were chosen as a target. Furthermore, a multi-wavelength sensor for a wide range of different pH values is introduced which is also based on the same system as probe **1**. Also, both derivatives can mimic Boolean operations like AND or INHIB[27–29] and even more advanced logic operations.

Results and discussion

Synthesis

Scheme 1 illustrates the synthetic pathway yielding compounds **1–4**. In the first step 1-pyrenol was selectively monobrominated at the distal ring. The mixture of both regioisomers **5** was subsequently transformed into the corresponding disulfonamides **6**. After the reaction with benzyl bromide, the two isomers could be separated by preparative

[a]*Biophysical Chemistry, Saarland University, Campus B2 2, 66123 Saarbrücken, Germany. E-mail: g.jung@mx.uni-saarland.de; Fax: +49 (0)681 302 64846; Tel: +49 (0)681 302 64848*

[b]*Fraunhofer-IBMT, Ensheimer Straße 48, 66386 St. Ingbert, Germany*

† This work is dedicated to Andreas Zumbusch on the occasion of his 50th birthday.

‡ Electronic supplementary information (ESI) available: Further compound characterization, determination of enzyme kinetics, further preliminary live-cell experiments and details for molecular logic. CCDC 1443123. For ESI and crystallographic data in CIF or other electronic format see DOI: 10.1039/c6pp00290k

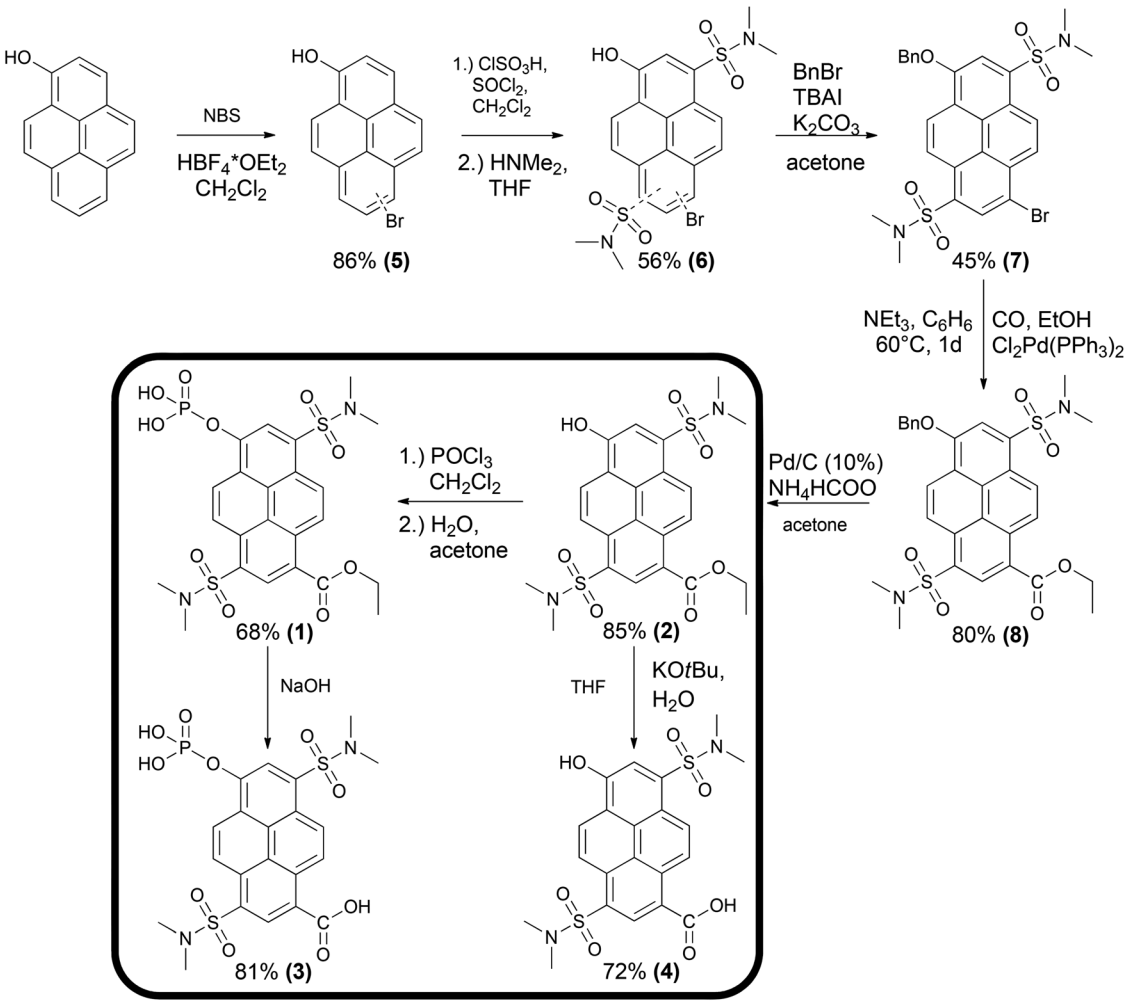

Scheme 1 Synthesis of **1–4**.

column chromatography. For further synthesis, solely derivative **7** was used, the substitution pattern of which was confirmed by X-ray crystallographic analysis (see ESI S17–S20‡). Subsequently, the bromine atom was transformed in a palladium-catalyzed carbonylation into the carboxylic ethyl ester **8**. The hydroxyl group was then deprotected *via* palladium-catalyzed transfer hydrogenation yielding **2**. The dual enzyme sensor **1** was synthesized by the reaction of **2** with phosphoroxy chloride and subsequent hydrolysis of the resulting dichloride in a water/acetone mixture in an overall yield of 10% over six steps. Additionally, the expected products of an enzymatic hydrolysis (**3** and **4**) were synthesized for comparison. The multi-wavelength pH-sensor compound **4** was obtained upon alkaline hydrolysis of **2** with potassium *tert*-butoxide in the presence of water according to the procedure of Gassman *et al.*[30] and compound **1** was hydrolyzed in a weakly alkaline aqueous solution to yield **3**.

Since the hydroxyl group and the opposite position of the aromatic system are the substitution sites inducing spectral changes to distinctly different extents, derivatives for other analytes can be created by variation of two of the six reaction steps (Scheme 1). Furthermore, compounds **1–4** exhibit high photostability (see ESI S38‡), long fluorescence lifetimes and quantum yields of at least 85% (Tables 1 and 3) which qualifies them as powerful tools for ultrasensitive fluorescence spectroscopy.

Table 1 Spectroscopic properties of **1–3** at physiological pH (pH = 8), for spectroscopy of **4** see Table 3, for other forms of **2**, see ESI S35

	1	**2** [a]	**3**
$\lambda_{max,abs}$ [nm]	410	484	407
$\lambda_{max,em}$ [nm]	472	558	448
Φ	0.98	0.86	1.00
$\tau_{fl,\ RO^-}$ [ns]	3.89	5.81	3.73

[a] RO^--form.

Dual enzyme substrate

Pyrenol and especially its sulfonated derivatives are classified as photoacids.[31–33] If these molecules are electronically excited, the observed fluorescence mainly results from the conjugated base formed by excited-state proton transfer (ESPT)

and is bathochromically shifted compared to the conjugated acid for electronic reasons. The corresponding base can also be excited directly at pH values above the ground state pK_a. Introduction of electron-withdrawing groups into the aromatic system is a common way to tune the photophysical properties of photoacids.[34–43] Hence, we introduced a cleavable carboxylic ester into the pyrene scaffold (**1** and **2**). The carboxylic ethyl ester (R-CO_2Et) exhibits a Hammett σ_p-value, a convenient measure of electron-withdrawing properties, of 0.45 [44] whereas carboxylate (R-CO_2^-) at a physiological pH is less electron-withdrawing (σ_p = 0.00).[44] Thus, fluorescence emission of the hydrolysis products (**3** and **4**) is blue shifted compared to **1** and **2**, respectively (Fig. 1). A substrate for phosphatases is obtained by conversion of the hydroxyl-group to a phosphate monoester (**1** and **3**). At physiological pH, hydrolysis of this group results in a strongly red shifted emission since the emission arises from the corresponding base of compound **2** or **4**, respectively (Fig. 1 and Table 1). Remarkably, the effects of phosphorylation and esterification are roughly additive on the wavelength scale.

Enzymatic hydrolysis of **1** by porcine liver esterase (PLE) shifts the emission from λ_{em} = 472 nm to λ_{em} = 448 nm. Upon dephosphorylation by alkaline phosphatase (AlP), fluorescence is shifted from λ_{em} = 472 to λ_{em} = 558 nm. When both enzymes are present, their combination induces an emission maximum at λ_{em} = 536 nm. Precise comparison of the spectroscopic data with the reference compounds **2–4** confirms that indeed these products are formed by the intended enzymatic reactions. Kinetic parameters of the enzyme reactions were determined *via* fluorescence spectroscopy using a Lineweaver–Burk plot (see ESI S39–S44‡). As reference substrates, commercially available 4-methylumbelliferyl phosphate (4-MUP)[45] and butyrate (4-MUBu),[46] respectively, were used. The determined K_m values for the enzymatic hydrolysis of 4-MUP by AlP (Table 2) under the used assay conditions are in a similar range as those determined by Fernley *et al.*[45]

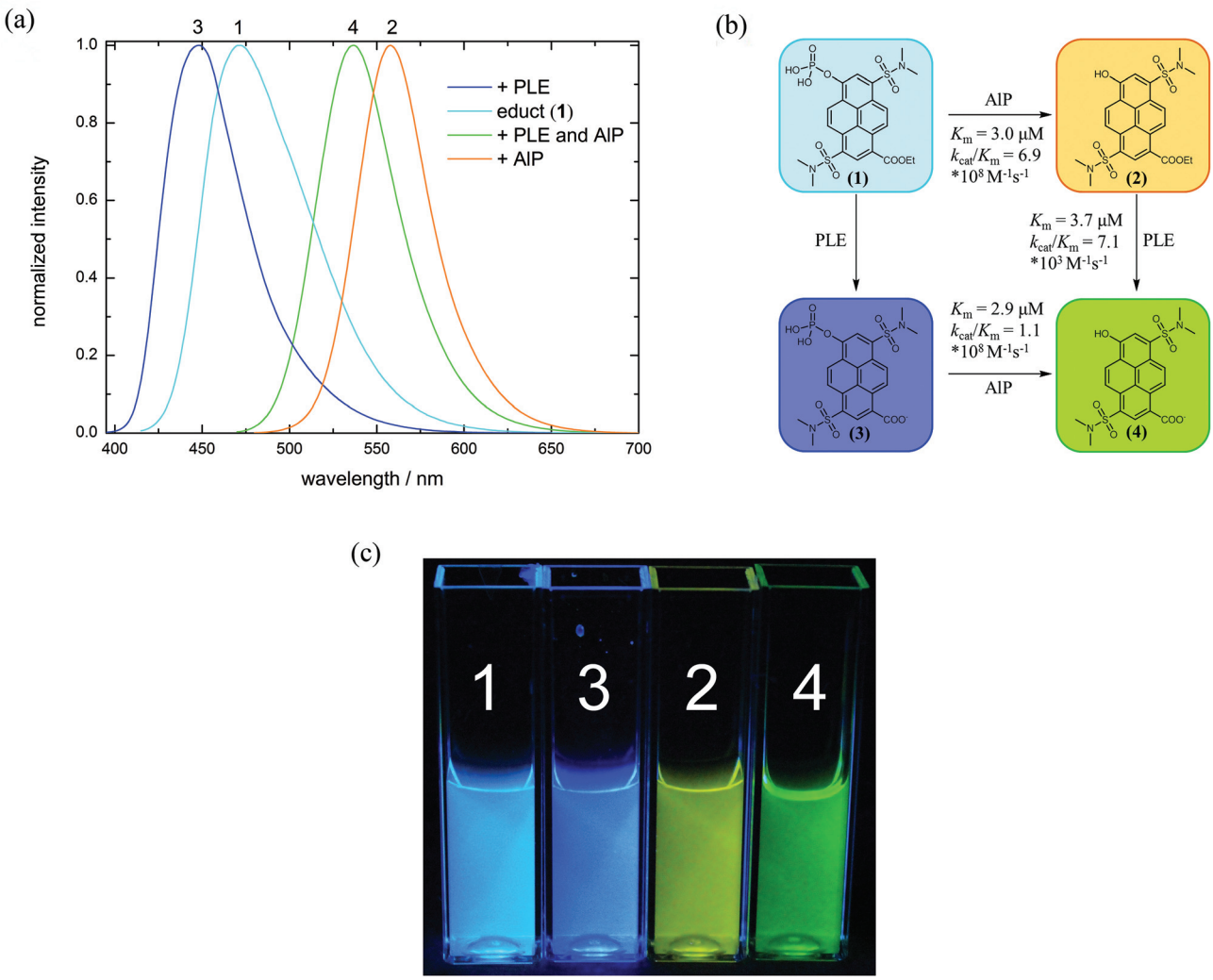

Fig. 1 (a) Normalized fluorescence emission of **1** (10^{-5} M, pH = 8) recorded 3 hours after incubation (enzymes in nanomolar concentration). (b) Schematic overview of spectral and molecular changes upon enzymatic conversion and the corresponding K_m and k_{cat}/K_m values. (c) Different metabolic states of **1**, visualized by backlight fluorescence excitation (λ_{ex} = 365 nm).

Table 2 Kinetic parameters for reactions of the dye system with different enzymes

Compound	1	3	4-MUP	1	3	2	4-MUBu
Enzyme	Alkaline phosphatase			Acid phosphatase		Porcine liver esterase	
K_m [μM]	3.0	2.9	2.2	40.8	48.6	3.7	16.9
k_{cat}/K_m [M^{-1} s^{-1}]	6.9×10^8	1.1×10^8	1.8×10^7	6.0×10^2	3.9×10^4	7.1×10^3	5.7×10^3

The determined K_m values (Table 2) characterize **1** (K_m = 3.0×10^{-6} M) and **3** (K_m = 2.9×10^{-6} M) as good substrates for alkaline phosphatase comparable to the fluorogenic reference compound 4-MUP under the same assay conditions (K_m = 2.2×10^{-6} M). The enzymatic efficiency of these probes, *i.e.* k_{cat}/K_m are also in a similar range as that found for 4-MUP (Table 2). Furthermore, the phosphate hydrolysis of **1** and **3** can also be achieved by acid phosphatase (AP). K_m values are generally about ten times higher compared to enzymatic hydrolysis with alkaline phosphatase, and k_{cat}/K_m is reduced by several orders of magnitude (Table 2).

K_m values for the ester hydrolysis of **2** by porcine liver esterase are lower by the factor 5 whereas k_{cat}/K_m is roughly 1.3 times higher compared to the 4-methylumbelliferyl substrate 4-MUBu (Table 2), which suggests that **2** is a somewhat better substrate than the commercial fluorogenic probe. While the hydrolysis of **2** to **4** by PLE is rather fast, hydrolysis of **1** to **3** by PLE is decelerated, thus disabling determination of K_m. Hydrolysis rates were similarly slow with carboxylic acid esterase from *Paenibacillus barcinonensis*, which suggests that **1** is not an ideal substrate for carboxylesterases. According to the widely used empirical model proposed by Jones *et al.*[47,48] only the large hydrophobic pocket provides enough space for binding the aromatic core of **1** and **2**. Compared to **2**, **1** is not only sterically more bulky, but also twice negatively charged, which likely causes repulsion from the hydrophobic pocket. As a result, substrate **1** might not be optimally coordinated at the active site and hence, the enzymatic hydrolysis may not be very effective. However, k_{cat}/K_m of AlP and PLE are ordered in such a way that the conversion of **1** → **2** → **4** can be easily tracked by fluorescence spectroscopy.

Live-cell application

The dual enzyme sensor **1** was applied to L929 cells (Fig. 2; for T84 cells, see ESI S45‡). Excitation of **1** and the corresponding metabolites was performed, as previously, with two-photon excitation (λ_{ex} = 800 nm).[43]

As control, cells were incubated with the different possible products of the enzymatic transformation (see ESI S46 and S47‡). Even 24 hours after incubation, no permeation in cells was found for compounds with the free carboxylate group (**3** and **4**), presumably due to the negative charge at this substituent. Besides the absence of membrane penetration of **4**, the corresponding image further shows that no significant autofluorescence was detectable under the used setup conditions. Interestingly, uptake of the negatively charged phosphoric acid monoester **1** into the cell plasma was detectable in each measurement. The transport inside might be facilitated by

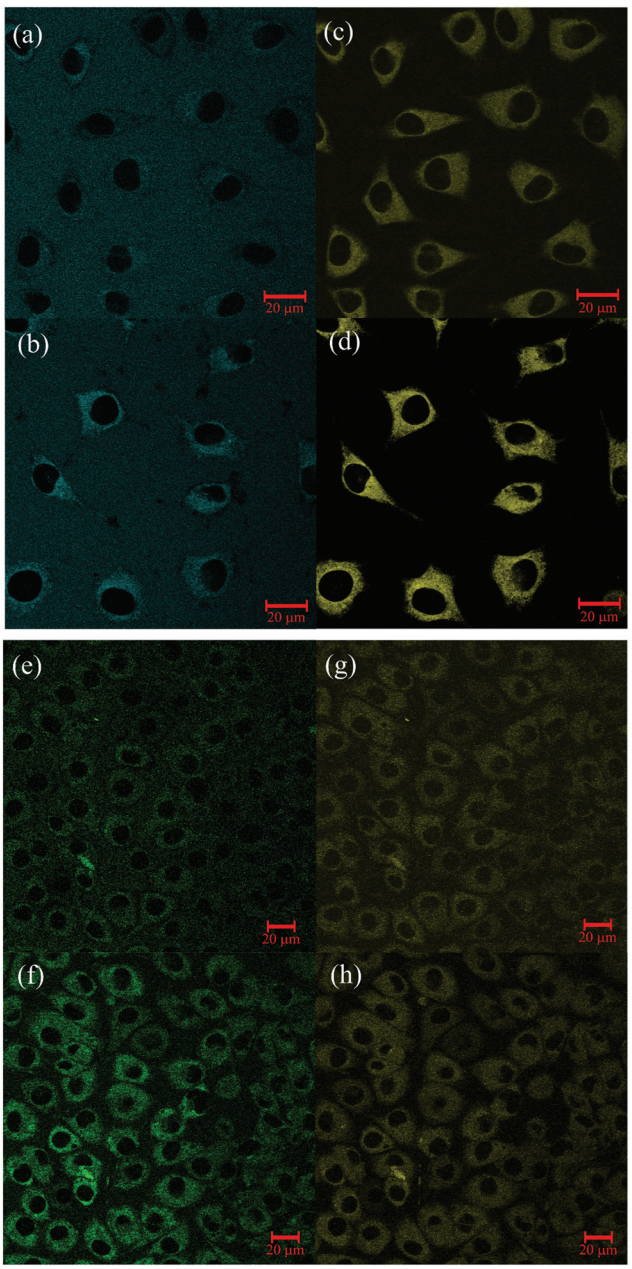

Fig. 2 Pseudo-colored fluorescence microscopic images of several cell clusters incubated with **1** and excited at λ_{ex} = 800 nm: (a–d) L929 cells, 1 h (a, c) and 3 h (b, d) after incubation, blue channel (a, b): λ_{det} = 435–485 nm (detection of compound **1**), yellow channel (c, d): λ_{det} = 535–612 nm (detection of compound **2**); (e–h) L929 cells, 1 h (e, g) and 3 h (f, h) after incubation, green channel (e, f): λ_{det} = 500–530 nm (detection of compound **4**), yellow channel (g, h): λ_{det} = 565–615 nm (detection of compound **2**).

transporter proteins which are naturally specialized in the exchange of nucleosides[49,50] through the cell membranes.

Fluorescence filters in Fig. 2(a, b) and (c, d) were selected to exclusively monitor the phosphatase activity. In the extracellular medium only emission of **1** is detected. After three hours, fluorescence emission of **1** is still detectable in the medium outside the cell, indicating an incomplete uptake and, moreover, the absence of segregated phosphatase. Detection of **1** within the cells suggests that metabolization occurs only after internalization. Emission of the dephosphorylated product **2** measured in the cytosol rises over time and reflects the intracellular phosphatase activity.

After conversion of **1** to **2**, the esterase activity was monitored by observation of the hydrolysis of **2** (λ_{det} = 565–615 nm) to **4** (λ_{det} = 500–530 nm). One hour after incubation with **1**, fluorescence from **2** is clearly discernible and emission of the hydrolyzed product **4** is only weakly detectable. While emission intensity of **2** was about the same after 3 hours (Fig. 2(g and h)), the fluorescence emission of **4** is much more pronounced (Fig. 2(e and f)). Similar behavior was previously observed in HeLa cells by use of a carboxyl BODIPY derivative.[16] Beneficially, k_{cat}/K_m of AlP and PLE (Table 2 and Fig. 1(b)) are ordered in such a way that the uptake and the subsequent conversion of **1** → **2** → **4** can be easily monitored by microscopy. It should be mentioned that **3** can only be detected when phosphatase activity is completely lacking. This is observed in selected areas of T84 cells (ESI Fig. S74‡).

The possible monitoring of the four distinct fluorescent products in the cell clusters enables the application of the above described concepts of molecular logic. For example, after incubation with **1**, the output of the green channel (λ_{det} = 500–530 nm, Fig. 2(e and f)) in combination with a suitable threshold value and the esterase/phosphatase activity as inputs represents an AND gate within the cell cluster similarly as previously shown.[22] In contrast to fluorogenic systems[22,51] our multi-wavelength probe additionally enables the read-out of more gates like INHIB (λ_{det} = 565–615 nm, Fig. 2(g and h)) without further effort, thus providing additional information. The use of all four detection wavelengths enables distinction of each metabolization state and allows for sensitive multiparameter sensing. As physicians often evaluate clinical parameters by binary read-out to draw a first diagnosis, the range of different molecular logic gates qualifies our device for multipurpose use in medical diagnostics.[52] This is actually possible without further technical tools as color changes are visible even by the naked human eye. In summary these first preliminary tests hint the use of **1** as a valuable tool for live-cell experiments, and other substrates with a broader application range are conceivable on the basis of Scheme 1.

Fluorescent multi-wavelength pH-sensor 4

Compound **4** contains two pH-sensitive groups which affect its spectral properties in a specific way (Fig. 3(b) and 5 and Table 3). The spectral variation is caused by the different emission of the photoacid (ROH) and the corresponding base (RO^-) and by the change of the electron-withdrawing properties by protonation/deprotonation of the carboxylic acid group (σ_p(R-CO_2H) = 0.45;[44] σ_p(R-CO_2^-) = 0.00 [44]). In contrast to compound **1**, where all the mutual combinations of substituents at the two orthogonal reaction sites are easily discernible (Fig. 1 (a and c)), only three states are visible in the emission spectra of **4** (Fig. 3(a)). The assignment of protonation states of **4a–d** to the emissive species relies on similar spectroscopic features of compounds **1–3**, where the substituents exhibit similar Hammett coefficients. Moreover, our interpretation also takes into account that the ordering of the acidities of the –OH and the –CO_2H groups likely is reversed upon excitation due to the pronounced photoacidity of aromatic alcohols and the photobasicity of aromatic carboxylates.[53–56] This peculiarity leads to the situation that **4d** is the stable monovalent form in the ground state whereas isomeric **4b** is only found in the excited

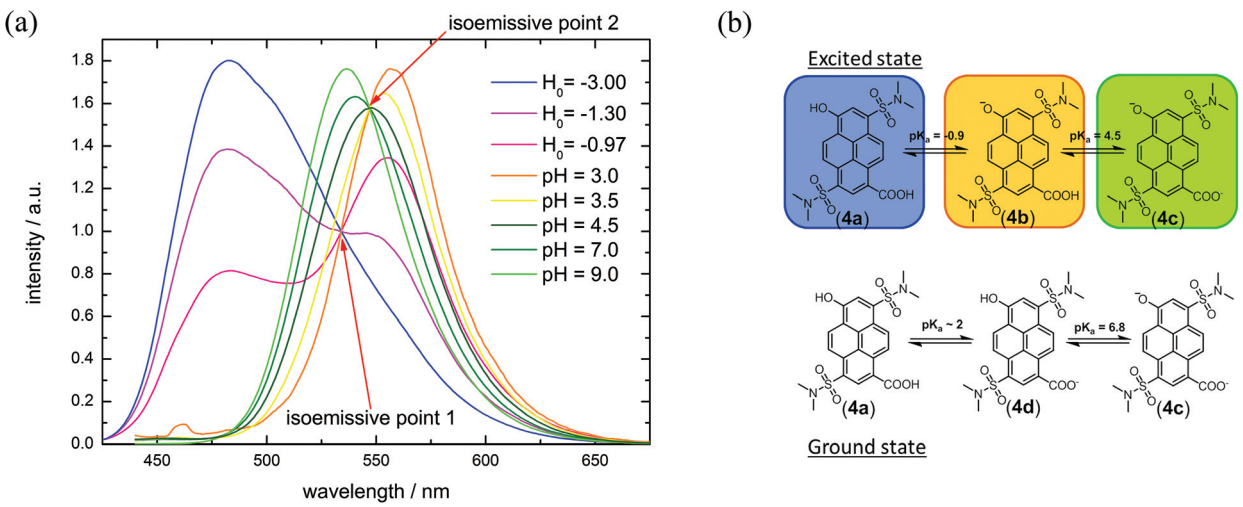

Fig. 3 (a) pH-Titration of compound **4** (λ_{ex} = 395 nm). (b) Different protonation states of **4** in the ground and excited states. The color refers to the spectra in (a).

Table 3 Spectroscopic data of compound **4**

	4
$\lambda_{max,abs}$ [nm]	418 (**4a**); 415 (**4d**); 463 (**4c**)
$\lambda_{max,em}$ [nm]	482 (**4a**); 557 (**4b**); 536 (**4c**)
pK_a [a]	6.8 (**ROH**CO_2^-); ~2.0 (RO^-**CO_2H**)
pK_a^* [b]	4.5 (ROH**CO_2H**); −0.9 (**ROH**CO_2H)
Φ	0.85 (**4c**)
$\tau_{fl,\ RO^-}$ [ns]	5.58

[a] Determined *via* absorption titration (for details, see ESI S32–S35). [b] Determined by fluorescence titration (for details, see ESI S32–S35).

state. Förster-calculations to estimate lacking acidity constants *e.g.* of **4d** or **4b** are therefore not yet possible.

At pH ≪ 0, fluorescence emission of compound **4** at λ_{em} = 482 nm (Fig. 3(b) and 5) results from the completely protonated excited species (**4a**). The excited-state acidity behind (pK_a^* = −0.9) agrees well with the value of **2** (pK_a^* = −0.8; Tables 1 and 3), evaluated by fluorescence titration (ESI S32 and S30‡),[57,58] and also lies in the range of that of HPTA (*N*,*N*,*N*′,*N*′,*N*″,*N*″-hexamethyl-1,3,6-trisulfonamide) (pK_a^* = −0.3).[43] Ongoing ESPT at pH values > 0 delivers the red shifted spectrum of the corresponding base (**4b**, λ_{em} = 557 nm). In this pH-range, *i.e.* 0 < pH < 4, no color change in the emission by conversion of **2** → **4** would be distinguishable because of the identical Hammett coefficients of the $-CO_2H$ and $-CO_2Et$ substituents. At pH > 5, the fluorescence emission shifts hypsochromically due to deprotonation of the carboxylic acid thus reducing the electron-withdrawing strength (**4c**, λ_{em} = 536 nm). Please note that the exact titration of the latter pK_a^*-values using fluorescence intensities is hampered by convolution of the respective molar extinction coefficients with the ground state equilibria. Anyway, the two mentioned underlying pK_a^*-values are experimentally accessible and are obtained from the trend of the depicted fluorescence titrations (Fig. 3(a); see also ESI Fig. S54, S55, S59 and S60‡), whereas the pK_a^*-values of the unstable isomeric form **4d** are not yet experimentally obtainable.

Conventional absorption titration experiments allow for the determination of the ground state pK_a-values (ESI Fig. S57 and S58‡). Above pH 6.8, **4** is primarily present in the double deprotonated form (**4c**) and the excitation maximum shifts from λ_{ex} = 415 nm (**4d**) to λ_{ex} = 463 nm (**4c**, Table 3). The fluorescence intensity at λ_{det} = 548 nm therefore drops from pH 6.5 to 11 due to weak excitation with light of the wavelength λ_{ex} = 395 nm (Fig. 5). A comparison with other pyrenol-derivatives provides insight into the electronic effects and supports our interpretation: structurally and electronically, **4** (as well as **2**) is a derivative of the photoacid HPTA.[42,43,59–62] This molecule contains a third *N*,*N*′-dimethyl sulfonamide group (σ_p = 0.65) which is more electron-withdrawing than the carboxylate resp. the ester in dye **4d** and **2**. As the influence of σ_p is reflected in the ground state acidity, the hydroxyl's pK_a of **2** and **4d** (pK_a = 6.6 and 6.8; Table 3) is about one logarithmic unit higher than that found for HPTA (pK_a = 5.6) but almost one unit below that of HPTS (8-hydroxypyrene-1,3,6-trisulfonic acid).[43,63] It should be mentioned that the difference of hydroxyl's pK_a-values between **2** and **4d** is less than expected, since the Hammett coefficients of the substituents (σ_p(R-CO_2Et) = 0.45; σ_p(R-CO_2^-) = 0.00) point to higher distinction. Indeed, the slightly lower pK_a-values obtained from FCS-experiments provide a larger difference (see ESI S37‡).

The second protonation equilibrium of **4a** due to deprotonation of the $-CO_2H$ moiety is less clearly defined in the absorption spectra. Only a minor spectral shift between pH 0 and 3 from λ_{abs} = 418 to 415 nm (ESI Fig. S56‡) prevents a reliable pK_a evaluation with absorption titration and provides only an estimate for the ground state pK_a-value of **4a**. Further experiments, including less ambiguous NMR-titrations with their demand for larger amounts of **4** and following the model by Ullmann,[64] represent current research. In particular, detection of the isomeric form **4b**, which appears to be less populated than in other systems,[65] and the associated protonation equilibria in the electronic ground state deserve exhaustive investigations. It is, however, yet unclear whether the excited-state acidity constant of **4d** can be experimentally found by time-resolved spectroscopy.

As the pK_a and pK_a^* of the hydroxyl and carboxyl groups are significantly different and the prevalent protonation states can be identified *via* fluorescence and/or absorption spectroscopy, compound **4** can be used as an optical sensor for a wide range of different pH values from highly acidic (pH < −1) to basic conditions (pH > 7). Four different pH-stages can be discriminated by optical spectroscopy due to the different spectral properties of species **4a–d**. While the pH values below −1 and between −0.5 and 4 resp. pH 5 and 6 can be identified *via* fluorescence spectroscopy, the pH-variation from 6 to 7 can be followed by a drop in fluorescence intensity (Fig. 5). This idea can also be transferred to the concept of molecular logic.

Molecular logic

Although many examples of molecular logic are already known, we demonstrate the diversity of our systems which can act as different gates or mimic more complex operations. As each metabolization state of **1** is characterized by a distinct fluorescence color and thus several different output channels can be observed, probe **1** in combination with different enzyme inputs represents a versatile tool for molecular logic. This system is able to perform simple Boolean logic operations like AND (**O4**), NOR (**O1**) and INHIB (**O2**, **O3**) (Fig. 4(a) and Table 4, for details see ESI S50–S58‡).[27–29,66–68] Additionally, OR and XOR gates can be constructed by the use of negative logic (see ESI S51 and S57‡).[69] The logic gate which is mimicked by the system is determined by selection of a suitable output channel wavelength and threshold value. In any of the mentioned examples, a buffer solution of **1** without any enzyme is defined as the initial state. By combination of several output channels and the two enzymes as input a 2:4 decoder,[70–72] 1:2 demultiplexer,[70,73,74] a half-adder[75–79] and -subtractor[69,78,79] and a transfer gate[70] (see ESI S49, S48, S59,

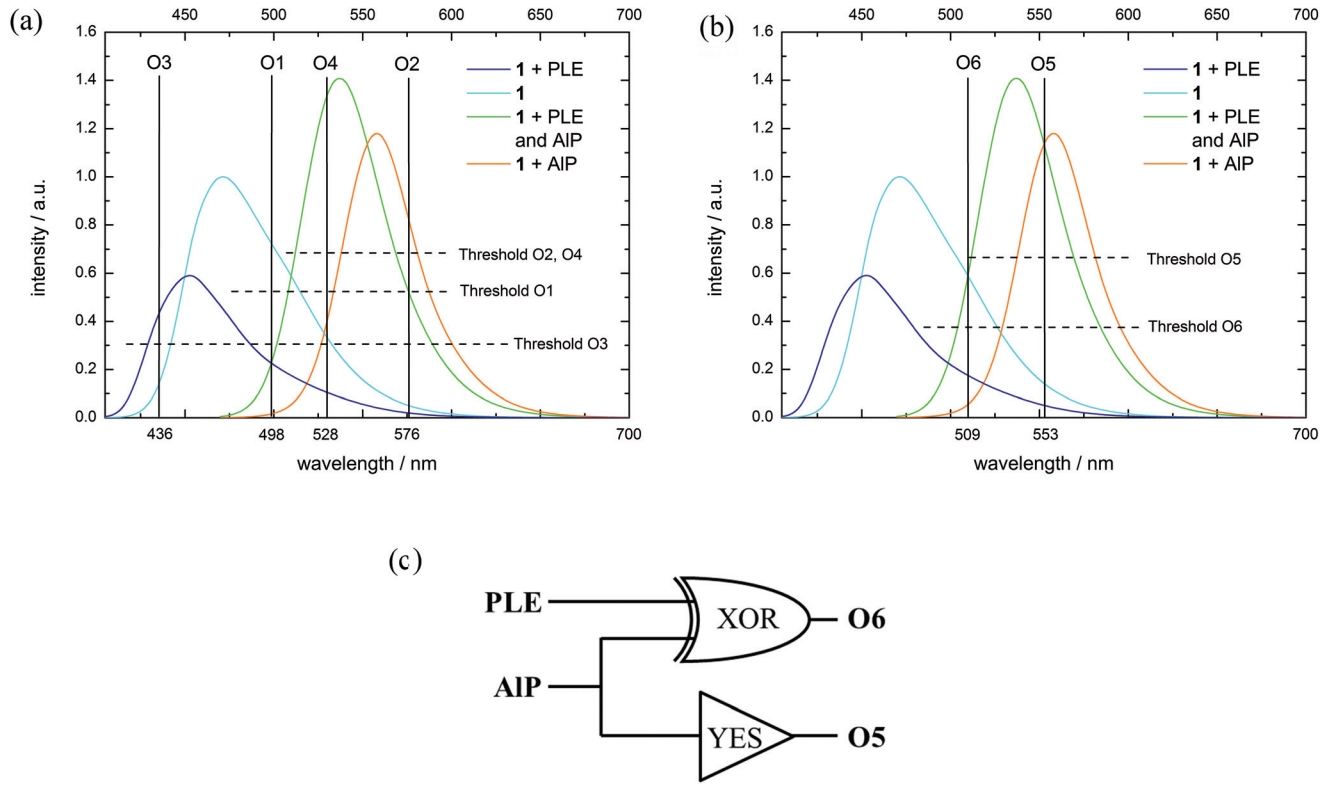

Fig. 4 (a) Fluorescence spectra (normalized to substrate fluorescence, λ_{ex} = 395 + 460 nm (see ESI S48‡), substrate concentration: 10^{-5} M, Tris-HCl buffer solution at pH = 8) with the corresponding output channels and threshold levels for (a) several logic operations (**O1–O4**) and (b) Feynman gate (**O5**, **O6**). (c) Logic circuit for the Feynman gate.

Table 4 Truth table for simple logic operations, 2:4 decoder (**O1–O4**) and Feynman gate (**O5**, **O6**) (λ_{ex} = 395 + 460 nm)

In1 (AlP)	**In2** (PLE)	**O1** (λ = 498 nm)	**O3** (λ = 436 nm)	**O2** (λ = 576 nm)	**O4** (λ = 528 nm)	**O5** (λ = 553 nm)	**O6** (λ = 509 nm, negative logic)
0	0	1	0	0	0	0	0
1	0	0	0	1	0	1	1
0	1	0	1	0	0	0	1
1	1	0	0	0	1	1	0
Gate (isolated)		**NOR**	**INHIB2**	**INHIB1**	**AND**	**YES**	**XOR**

S60 and S56‡) can be implemented. Furthermore, a molecular keypad lock[70,80–86] is realized by the use of acid phosphatase, potassium hydroxide and excitation light as input (see ESI S62‡).

To exemplify some logic operations, the use of **1** as a 2:4 decoder is explained in more detail. A 2:4 decoder translates binary information from two encoded (**In1**, **In2**) inputs to four unique outputs (**O1–O4**).[71] The truth table for this information processor is shown in Table 4. In the initial state, only **O1** is on due to the fluorescence emission of **1**. When either AlP (**In1**) or PLE (**In2**) is added, the substrate is converted into the corresponding product, which means that the substrate (**1**) fluorescence vanishes (**O1** = off) and solely the fluorescence of the formed dye is monitored (**O2** = on resp. **O4** = on). If both inputs are present, compound **4** is generated and the fluorescence at output channel **O4** exceeds the threshold value, while all other output channels are off.

Reversible molecular logic was achieved with a Feynman gate (Fig. 4(b and c) and Table 4, see ESI S61‡). Here, **O5** represents the control output for the AlP input (YES-gate) and **O6** acts as an XOR gate for AlP and PLE (target output). While the fluorescence emission at **O5** only exceeds the corresponding threshold value when AlP is present, the simultaneous absence or presence of both PLE and AlP yields an emission at **O6** above the corresponding threshold. As output of **O6** is treated as negative logic, the XOR-like behavior is realized. The combination of these both gates to the Feynman gate generates a unique output pattern for each input.

Although the presented system can process information in a logically reversible way, it is not resettable since **1** is irreversibly metabolized by the enzymes. Many resettable systems with a chelating motif use ions as input. However, resetting the system in its initial state usually requires removal of the ions with additional effort.[78,87] Alternative resettable systems use photons[70,71,81,88] or pH-variation as input.[77–79,89] In the latter case, H^+ and OH^- are used as inputs and the system becomes resettable, since these inputs can annihilate each other.[78]

In combination with definite amounts of H^+ and/or OH^- as input and a particular output wavelength, the pH-dependent fluorescence changes of **4** allow for mimicking nearly every simple logic operation (see ESI S63–S71‡). Moreover, the system can be applied as a half-adder, half-subtractor and comparator[80,90] (see ESI S72–S74‡). In each of these applications, the system can be reset by addition of acid or base.

In the mentioned operation examples, the inputs are either chemically indistinguishable (the same amounts of H^+ *or* OH^-) or can fully annihilate each other (the same amounts of H^+ *and* OH^-). However, a reversible logic operation is achieved by choosing two different concentrations of base as input to create a Feynman gate (Fig. 5 and Table 5). While **O I** in the negative logic mode represents the YES gate for **In I** (low amount of OH^-), **O II** mimics an XOR gate for **In I** and **In II** (higher amount of OH^-). In the initial state at pH < 0, the emission above the threshold value at **O I** causes an on-response which is inverted by the negative operation to off. The same is true for the addition of **In II**, which sets the system to pH 6.5. Each other scenario causes an off response which is converted to on. **O II** only processes an on-signal after **In I** or **In II** addition (pH 3.5 or ~6.5, Fig. 5 and Table 5).

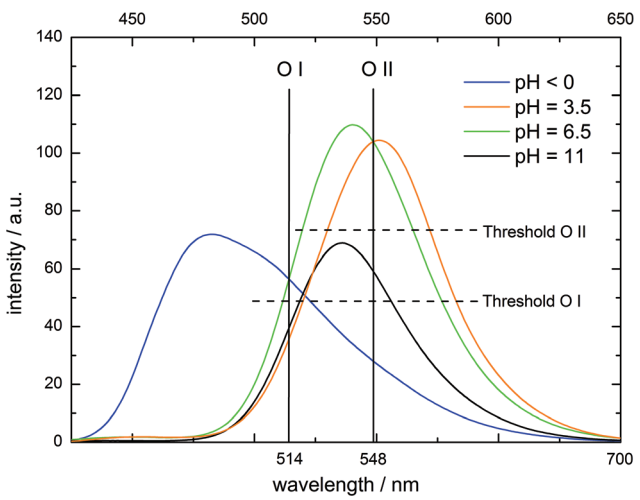

Fig. 5 Fluorescence emission of **4** at different pH values (λ_{ex} = 395 nm), output channels and the corresponding threshold values for molecular logic.

Table 5 Truth table for operation of **4** as Feynman gate (λ_{ex} = 395 nm)

In I (low amount OH^-)	**In II** (high amount OH^-)	**O I** (λ = 514 nm, neg. logic)	**O II** (λ = 548 nm)
0	0	0	0
1	0	1	1
0	1	0	1
1	1	1	0
Gate (isolated)		**YES**	**XOR**

Conclusion and outlook

The dual enzyme probe **1** constitutes an efficient tool for monitoring orthogonal enzymatic activities producing four distinct emission colors which are distinguishable even by the naked human eye. It can act as an individual probe for two different enzymes, allowing for their identification on the basis of different fluorescence colors, and can indicate the presence of both enzymes as well. Internal referencing in a ratiometric way is enabled by the fluorescent substrate.

Compound **4** can be used as a multi-wavelength sensor for a wide range of different pH values as the protonation states can be distinguished by their spectral properties. Furthermore, the two multi-wavelength ratiometric pyrene derivatives can be used for different applications of molecular logic. Beyond simple Boolean logic, both derivatives **1** and **4** are capable of more complex operations. Moreover, both systems can operate in a logically reversible way thus preventing information loss, and **4** can even be reset. Suchlike operation of **4** as a non-trivial Feynman gate appears promising in view of our own attempts to combine chemistry with quantum optics.[91,92] The described synthesis allows for a modification of pyrenol into a multi-wavelength probe for other analytes or macromolecules. Since the color of the fluorescence emission strongly relies on the substitution of the hydroxyl group (position 6) by enabling or disabling deprotonation and to a minor extent on the opposite position (position 1), more derivatives with orthogonal reactivities will be available. In summary, the described pyrenol derivatives present a versatile, flexible and chameleonic platform for the multianalyte probing and molecular logic in life science and chemistry.

Experimental section

UV/Vis and fluorescence spectroscopy

Absorption spectra were recorded with a Jasco Spectrophotometer V-650, and fluorescence emission and excitation spectra were recorded with a Jasco Spectrofluorometer FP-6500. Concentrations of the measured solutions were in the micromolar range if not stated otherwise.

Enzyme kinetics

All enzymatic *in vitro* reactions were examined at 25 °C in aqueous buffer solution (0.1 M Tris-HCl at pH 8.0 for alkaline phosphatase (AlP) and porcine liver esterase (PLE); 0.1 M acetate at pH 5.0 for acid phosphatase (AP)). Esterase from porcine liver (activity = 18 units per mg solid) and acid

phosphatase from potato (3.3 units per mg solid) were obtained as lyophilized powder from Sigma-Aldrich. Alkaline phosphatase from bovine intestinal mucosa in buffered aqueous solution (3.0 M NaCl, 0.2 mM $MgCl_2$, 30 mM triethanolamine, pH 7.6) with an activity of 3408 units per mg protein was also obtained from Sigma-Aldrich. Kinetic parameters were determined *via* fluorescence spectroscopy using a Lineweaver–Burk plot. Substrate concentrations were in the range of 0.1–25 μM and enzyme concentration was in the picomolar range in the case of AlP and in the nanomolar range in that of PLE and AP. For determination of the kinetics, the decrease of the substrate fluorescence was monitored. When evolution of the product fluorescence is recorded, the observed kinetics were found to be nearly the same. Details can be found in the ESI S39–S45.‡

Two-photon excitation laser scanning microscopy

Laser scanning microscopy was performed with a confocal laser microscope (LSM510 META, Zeiss; Objective: Plan-Neofluar 40×/1.3, Zeiss). Excitation was performed with a Ti:Sa laser (Chameleon XR, Coherent) operating at λ = 800 nm.

Cell cultures

T84 cells were grown in a 1 : 1 mixture of Ham's F12 medium and Dulbecco's modified Eagle's medium with 2.5 mM 95% L-glutamine and 5% fetal bovine serum before incubation at 37 °C, 5% CO_2 for 1–2 days. Before the experiment, the cells were washed with a 0.25% (w/v) trypsin–0.53 mM EDTA solution to remove all traces of serum that contains a trypsin inhibitor. L929 cells were grown in Eagle's Minimum Essential Medium modified to contain Earle's Balanced Salt Solution with non-essential amino acids, 2 mM L-glutamine, 1 mM sodium pyruvate, and 1500 mg L^{-1} sodium bicarbonate containing horse serum to a final concentration of 10% prior incubation at 37 °C, 5% CO_2 for 1–2 days. Before the experiment, the cells were washed with a 0.25% (w/v) trypsin–0.53 mM EDTA solution to remove all traces of serum that contains a trypsin inhibitor. For incubation, compounds **1** and **3** were dissolved in water and dyes **2** and **4** were dissolved in DMSO.

Synthetic procedures: general

All reagents and solvents were obtained from Sigma-Aldrich, Merck or Acros Organics and used without further purification. For the chromatographic purification of compound **4**, silica gel was washed prior to use with an 8 : 2 (v/v) mixture of methylene chloride/methanol and then dried *in vacuo*. Pyrenol was synthesized according to a modified procedure of Sehgal *et al.*[93]

^{1}H- and ^{13}C-NMR spectra were recorded with a Bruker AM 400 spectrometer operating at 400 and 100 MHz, respectively. Alternatively, a Bruker AM 500 spectrometer operating at 500 and 125 MHz, respectively, was used.

HRMS spectra were recorded with a Bruker solariX 7 Tesla instrument equipped with an Infinity Cell.

Data for X-ray structure determination were collected on an X8 ApexII X-ray diffractometer operating with MoKα radiation. Further details of the crystal data and structure refinement are gathered in Tables S1 and S2 in the ESI.‡

6- and 8-bromopyren-1-ol (5). Pyrenol (120.0 mg, 0.55 mmol) was dissolved in absolute acetonitrile (20 mL) and cooled to −35 °C. Subsequently, tetrafluoroboric acid diethyl ether complex (98.2 mg, 0.61 mmol) was introduced to the solution, and *N*-bromosuccinimide (107.6 mg, 0.61 mmol) was added in small portions. After stirring for 18 hours and warming to room temperature, the resultant black mixture was diluted with $NaHSO_3$ solution (38%, 30 mL) and stirred for an additional 15 minutes. Diethylether (40 mL) was added and the resulting mixture was washed three times with water (40 mL) and once with saturated NaCl (40 mL) solution, before the organic phase was dried over sodium sulfate. After evaporation of the solvent, the crude product was purified *via* column chromatography (diethylether/petrol. ether 40–65 = 4 : 6 (v/v)) and a mixture of 6- and 8-bromopyren-1-ol was obtained as a white solid (142.0 mg, 0.48 mmol, 86%). UV/Vis (DMSO): λ_{max} = 358 nm, (DMSO + NaOH): λ_{max} = 472 nm; fluorescence (DMSO): λ_{max} = 399 nm, (DMSO + NaOH): λ_{max} = 477 nm. 6-Bromopyren-1-ol: ^{1}H-NMR (400 MHz, acetone-d6, 25 °C): δ = 9.68 (1H, s, OH), 8.58 (1 H, d, ^3J(H,H) = 9.6 Hz, Ar–*H*), 8.30 (1 H, d, ^3J(H,H) = 9.6 Hz, Ar–*H*), 8.22–8.14 (2 H, m, Ar–*H*), 8.05–8.01 (2 H, m, Ar–*H*), 7.88 (1 H, d, ^3J(H,H) = 9.0 Hz, Ar–*H*), 7.69 ppm (1 H, d, ^3J(H,H) = 8.5 Hz, Ar–*H*). ^{13}C-NMR (100 MHz, acetone-d6, 25 °C): δ = 153.5, 132.6, 131.1, 131.0, 130.3, 128.9, 128.1, 127.2, 126.3, 125.8, 124.8, 124.7, 124.3, 119.5, 118.6, 114.8 ppm. 8-Bromopyren-1-ol: ^{1}H-NMR (400 MHz, acetone-d6, 25 °C): δ = 9.67 (1H, s, OH), 8.48 (1 H, d, ^3J(H,H) = 9.3 Hz, Ar–*H*), 8.22–8.14 (4 H, m, Ar–*H*), 8.05–8.01 (2 H, m, Ar–*H*), 7.68 ppm (1 H, d, ^3J(H,H) = 8.3 Hz, Ar–*H*). ^{13}C-NMR (100 MHz, acetone-d6, 25 °C): δ = 153.7, 132.5, 131.1, 131.0, 127.8, 127.1, 126.4, 126.3, 125.6, 125.5, 125.4, 123.2, 122.8, 119.7, 118.9, 114.8 ppm. MS (ESI): *m*/*z* calc. for $C_{16}H_9BrO$: 294.975852 $[M - H]^-$, found: 294.97555.

3-Bromo-8-hydroxy-*N*,*N*,*N*′,*N*′-tetramethylpyrene-1,6-disulfonamide and 3-bromo-6-hydroxy-*N*,*N*,*N*′,*N*′-tetramethylpyrene-1,8-disulfonamide (6). A mixture of regioisomers **5** (100.0 mg, 0.34 mmol) was dissolved in dry methylene chloride (20 mL) and cooled to −10 °C. Chlorosulfonic acid (392.1 mg, 3.37 mmol) was added slowly and the resultant mixture was stirred for 18 hours upon warming up to room temperature. After addition of thionyl chloride (200.5 mg, 1.69 mmol), the black slurry was heated to reflux for five hours. Before removal of the solvent and excessive thionyl chloride *in vacuo*, the resulting solution was cooled down to room temperature. After addition of dry THF (20 mL) to the residue and cooling to −10 °C, dimethylamine dissolved in THF (1 M, 10 mL) was added to the resulting solution. The reaction mixture was stirred for 18 hours, ethyl acetate was added and the organic phase was washed three times with hydrochloric acid (1 M, 40 mL) and saturated NaCl solution (40 mL) before being dried over sodium sulfate. Subsequently, the solvent was evaporated and the crude product was purified by column chromatography (ethyl acetate/petrol. ether 40–65 = 6 : 4 (v/v)) to yield the isomer mixture **6** (96.1 mg, 0.19 mmol, 56%) as a

yellow powder. UV/Vis (DMSO + TFA): λ_{max} = 432 nm, (DMSO): λ_{max} = 532 nm; fluorescence (DMSO; DMSO + TFA): λ_{max} = 450 nm, (DMSO): λ_{max} = 532 nm. 3-Bromo-6-hydroxy-*N*,*N*,*N*′,*N*′-tetramethylpyrene-1,8-disulfonamide: ^{1}H-NMR (400 MHz, acetone-d6, 25 °C): δ = 10.54 (1H, s, OH), 9.36 (1 H, d, ^3J(H,H) = 9.6 Hz, Ar–*H*), 9.23 (1 H, d, ^3J(H,H) = 9.6 Hz, Ar–*H*), 8.86 (1 H, s, Ar–*H*), 8.79 (1 H, d, ^3J(H,H) = 9.6 Hz, Ar–*H*), 8.50 (1 H, d, ^3J(H,H) = 9.6 Hz, Ar–*H*), 8.38 (1 H, s, Ar–*H*), 2.90 (6 H, s, 2 CH_3), 2.87 ppm (6 H, s, 2 CH_3). ^{13}C-NMR (100 MHz, acetone-d6, 25 °C): δ = 153.9, 134.1, 133.8, 133.3, 131.5, 130.3, 129.4, 127.3, 126.8, 125.7, 125.1, 124.4, 122.7, 122.5, 119.5, 116.9, 38.1 (2C), 38.0 (2C) ppm. 3-Bromo-8-hydroxy-*N*,*N*,*N*′,*N*′-tetramethylpyrene-1,6-disulfonamide: ^{1}H-NMR (400 MHz, acetone-d6, 25 °C): δ = 10.54 (1H, s, OH), 9.27 (1 H, d, ^3J(H,H) = 10.0 Hz, Ar–*H*), 9.08 (1 H, d, ^3J(H,H) = 10.0 Hz, Ar–*H*), 8.86 (1 H, s, Ar–*H*), 8.85 (1 H, d, ^3J(H,H) = 9.6 Hz, Ar–*H*), 8.61 (1 H, d, ^3J(H,H) = 9.6 Hz, Ar–*H*), 8.38 (1 H, s, Ar–*H*), 2.91 (6 H, s, 2 CH_3), 2.88 ppm (6 H, s, 2 CH_3). ^{13}C-NMR (100 MHz, acetone-d6, 25 °C): δ = 153.9, 134.6, 134.3, 133.9, 131.5, 133.4, 131.7, 129.3, 127.5, 127.3, 126.8, 126.5, 123.5, 122.1, 119.5, 116.9, 38.1 (2C), 38.0 (2C) ppm. MS (ESI): *m*/*z* calc. for $C_{20}H_{19}BrN_2O_5S_2$: 508.984052 $[M - H]^-$, found: 508.98384.

3-(Benzyloxy)-8-bromo-*N*,*N*,*N*′,*N*′-tetramethylpyrene-1,6-disulfonamide (7). Sodium carbonate (329.4 mg, 2.28 mmol) and tetrabutylammonium iodide (TBAI) (17.2 mg, 0.05 mmol) were added to a solution of the isomer mix **6** (221.6 mg, 0.43 mmol) in dry acetone (50 mL). After addition of benzyl bromide (96.5 mg, 0.56 mmol), the orange solution was stirred for 42 hours at room temperature. The solvent was removed, methylene chloride (40 mL) was added and the organic phase was washed three times with hydrochloric acid (1 M, 40 mL) and saturated NaCl solution (40 mL) before drying over sodium sulfate. Column chromatography (methylene chloride/petrol. ether 40–65 = 9 : 1 (v/v)) was used to purify the crude mixture of the resulting regioisomers and yielded **7** as a yellow powder (116.7 mg, 0.19 mmol, 45%). UV/Vis (DMSO): λ_{max} = 420 nm; fluorescence (DMSO): λ_{max} = 436 nm. ^{1}H-NMR (400 MHz, chloroform-d, 25 °C): δ = 9.26 (1 H, d, ^3J(H,H) = 9.8 Hz), 9.27 (1 H, d, ^3J(H,H) = 9.19 Hz, Ar–*H*), 8.93 (1 H, s, Ar–*H*), 8.82 (1 H, d, ^3J(H,H) = 9.8 Hz, Ar–*H*), 8.49 (1 H, d, ^3J(H,H) = 9.8 Hz, Ar–*H*), 8.32 (1 H, s, Ar–*H*), 7.5 (5 H, m, Ar–*H*), 5,58 (2 H, s, CH_2), 2.89 (6 H, s, 2 CH_3), 2.72 ppm (6 H, s, 2 CH_3). ^{13}C-NMR (100 MHz, chloroform-d, 25 °C): δ = 152.8, 135.8, 132.9, 132.8, 131.8, 130.6, 128.9 (2C), 128.8, 128.5, 127.9, 127.5 (3C), 126.2, 125.6, 125.4, 123.5, 123.3, 122.7, 119.8, 112.9, 71.3, 37.6 (2C), 37.5 (2C) ppm. MS (ESI): *m*/*z* calc. for $C_{27}H_{25}BrN_2O_5S_2$: 623.028043 $[M + Na]^+$, found: 623.02891.

Ethyl 6-(benzyloxy)-3,8-bis(*N*,*N*-dimethylsulfamoyl)pyrene-1-carboxylate (8). Compound **7** (64.5 mg, 0.11 mmol) was dissolved in a reaction tube with a mixture of benzene (9.29 mL), triethylamine (3.44 mL) and ethanol (1.82 mL). Before the tube was introduced in the autoclave, $[Pd(PPh_3)_2Cl_2]$ was added to the reaction mixture which then was heated to 65 °C for 12 hours under a CO pressure of 16 bar. The solution was cooled to room temperature and transferred to a 100 mL flask, the solvent was removed and the residue was dissolved in methylene chloride (30 mL). Before being dried over sodium sulfate and evaporation of the solvent, the organic phase was washed three times with water (30 mL) and saturated NaCl solution (30 mL). Compound **8** was obtained as a yellow powder after column chromatography (methylene chloride/petrol. ether 40–65 = 9 : 1 (v/v)) in a yield of 80% (48.9 mg, 0.09 mmol). UV/Vis (DMSO): λ_{max} = 420 nm; fluorescence (DMSO): λ_{max} = 462 nm. ^{1}H-NMR (400 MHz, chloroform-d, 25 °C): δ = 9.24 (4 H, m, Ar–*H*), 8.91 (1 H, ^3J(H,H) = 9.6 Hz Ar–*H*), 8.32 (1 H, s, Ar–*H*), 7.47 ppm (5 H, m, Ar–*H*), 5.59 (2 H, s, CH_2), 4.61 (2H, q, ^3J(H,H) = 7.3 Hz, CH_2), 2.90 (6 H, s, 2 CH_3), 2.73 (6 H, s, 2 CH_3), 1.55 ppm (3H, t, ^3J(H,H) = 7.3 Hz, CH_3). ^{13}C-NMR (100 MHz, chloroform-d, 25 °C): δ = 166.6, 153.2, 135.7, 135.0, 133.9, 132.5, 131.9, 131.1, 130.5, 129.5, 128.9, 128.5, 128.0, 127.5, 125.8, 125.7, 125.2, 125.0, 124.2, 123.9, 123.2, 122.1, 112.7, 71.3, 62.0, 37.5 (4C), 14.4 ppm. MS (ESI): *m*/*z* calc. for $C_{30}H_{30}N_2O_7S_2$: 617.138661 $[M + Na]^+$, found: 617.13953.

Ethyl 3,8-bis(*N*,*N*-dimethylsulfamoyl)-6-hydroxypyrene-1-carboxylate (2). In a 100 mL flask equipped with a reflux condenser and a gas bubbler, ammonium formate (223.4 mg, 63.1 mmol) and palladium on carbon (10 wt%, 360 mg) were added to a solution of **8** (202.2 mg, 0.35 mmol) in acetone (40 mL). The reaction suspension was heated to reflux. When the evolution of gas ceased, the mixture was stirred for an additional hour. After cooling to room temperature, the suspension was filtered through a plug of celite and the solvent of the resulting solution was evaporated. The residue was dissolved in ethyl acetate (40 mL), washed three times with hydrochloric acid (1 M, 40 mL) and saturated NaCl solution (40 mL) and dried over sodium sulfate. Column chromatography (ethyl acetate/petrol. ether 40–65 = 6 : 4 (v/v)) of the raw product yielded **2** as a yellow powder (143.0 mg, 0.30 mmol, 85%). UV/Vis (DMSO + TFA): λ_{max} = 426 nm, (DMSO): λ_{max} = 559 nm, (H_2O + HCl): λ_{max} = 419 nm, (H_2O): λ_{max} = 494 nm; $\varepsilon_{(494)}$ (H_2O, RO^-) = 25 000 L mol^{-1} cm^{-1}; fluorescence (DMSO + TFA): λ_{max} = 482/576 nm, (DMSO): λ_{max} = 576 nm, (H_2O + HCl): λ_{max} = 478 nm, (H_2O): λ_{max} = 558 nm. ^{1}H-NMR (500 MHz, acetone-d6, 25 °C): δ = 9.34 (1 H, d, ^3J(H,H) = 10.0 Hz, Ar–*H*), 9.28 (1 H, d, ^3J(H,H) = 9.4 Hz, Ar–*H*), 9.25 (1 H, ^3J(H,H) = 10.0 Hz, Ar–*H*), 9.21 (1 H, s, Ar–*H*), 8.88 (1 H, d, ^3J(H,H) = 9.4 Hz, Ar–*H*), 8.38 (1 H, s, Ar–*H*), 4.60 (2H, q, ^3J(H,H) = 7.3 Hz, CH_2), 2.89 (6 H, s, 2 CH_3), 2.88 (6 H, s, 2 CH_3), 1.53 ppm (3 H, t, ^3J(H,H) = 7.3 Hz, CH_3). ^{13}C-NMR (125 MHz, acetone-d6, 25 °C): δ = 167.3, 154.3, 134.7 (2C), 132.2, 131.8, 130.4, 129.2, 127.1, 126.8, 126.0, 125.6, 124.6, 124.0, 122.4, 122.1, 116.8, 62.6, 38.1 (2C), 38.0 (2C), 14.8 ppm. MS (ESI): *m*/*z* calc. for $C_{23}H_{24}N_2O_7S_2$: 503.09467 $[M - H]^-$, found: 503.09282.

3,8-Bis(*N*,*N*-dimethylsulfamoyl)-6-hydroxypyrene-1-carboxylic acid (4). Compound **2** (17.8 mg, 0.04 mmol) was dissolved in dry THF (10 mL) to which was then added water (3.06 mg, 0.17 mmol) and potassium *tert*-butoxide (83.04 mg, 0.74 mmol). The reaction mixture was stirred for 24 hours at room temperature, before the addition of ethyl acetate (20 mL). Subsequently, the organic phase was washed three times with hydrochloric acid (1 M, 20 mL) and saturated NaCl

solution (20 mL) and dried over sodium sulfate. **4** was purified with column chromatography (methylene chloride/methanol = 9 : 1 (v/v)) to give a yellow powder (12.6 mg, 0.03 mmol, 72%). UV/Vis (DMSO + TFA): λ_{max} = 425 nm, (DMSO): λ_{max} = 424/557 nm, (H_2O + HCl): λ_{max} = 415/418 nm, (H_2O): λ_{max} = 463 nm; $\varepsilon_{(463)}$ (H_2O, RO^-) = 17 000 L mol^{-1} cm^{-1}; fluorescence (DMSO + TFA): λ_{max} = 476/573 nm, (DMSO): λ_{max} = 573 nm, (H_2O + HCl): λ_{max} = 482 nm, (H_2O): λ_{max} = 536/557 nm. ^{1}H-NMR (500 MHz, acetone-d6, 25 °C): δ = 9.38 (1 H, d, ^3J(H,H) = 10.0 Hz, Ar–*H*), 9.24 (1 H, d, ^3J(H,H) = 9.6 Hz, Ar–*H*), 9.20 (1 H, ^3J(H,H) = 10.0 Hz, Ar–*H*), 9.16 (1 H, s, Ar–*H*), 8.79 (1 H, d, ^3J(H,H) = 9.6 Hz, Ar–*H*), 8.34 (1 H, s, Ar–*H*), 2.88 (6 H, s, 2 CH_3), 2.85 ppm (6 H, s, 2 CH_3). ^{13}C-NMR (125 MHz, acetone-d6, 25 °C): δ = 179.3, 153.8, 134.1, 133.7, 132.1, 131.7, 130.0, 128.8, 127.9, 127.2, 126.0, 125.6, 125.4, 125.0, 122.4, 122.2, 116.3, 38.1 (2C), 38.0 (C2). MS (ESI): *m*/*z* calc. for $C_{21}H_{20}N_2O_7S_2$: 475.06337 $[M - H]^-$, found: 475.06494.

Ethyl 3,8-bis(*N*,*N*-dimethylsulfamoyl)-6-(phosphonooxy) pyrene-1-carboxylate (1). After dissolving phosphoroxy chloride (140 μL) in dry methylene chloride (40 mL) and cooling to −10 °C, a solution of **2** (48.1 mg, 0.10 mmol) and trimethylamine (40 μL) in dry methylene chloride (20 mL) was added slowly. The resulting, nearly colorless solution was stirred for 18 hours upon warming up slowly to room temperature. Water (3 mL) was added slowly and the mixture was stirred for an additional 10 minutes. The organic phase was washed three times with cooled water (~5 °C, 40 mL) and one time with saturated NaCl solution (~5 °C, 40 mL) before drying over sodium sulfate. After evaporation of the solvent, the raw dichlorophosphate was dissolved in a mixture of water (5 mL) and acetone (5 mL). Hydrolysis was monitored by using RP-TLC and was complete after 48 hours. The reaction mixture was extracted three times with ethyl acetate and the aqueous phase was dried *in vacuo*. Reverse phase column chromatography (water/methanol = 1 : 1 (v/v)) of the crude product yielded **1** as a yellow powder (37.6 mg, 0.07 mmol, 68%). UV/Vis (H_2O): λ_{max} = 410 nm; $\varepsilon_{(410)}$ (H_2O) = 19 300 L mol^{-1} cm^{-1}; fluorescence (H_2O): λ_{max} = 472 nm. ^{1}H-NMR (500 MHz, methanol-d4, 25 °C): δ = 9.35 (1 H, d, ^3J(H,H) = 10.0 Hz, Ar–*H*), 9.30 (1 H, d, ^3J(H,H) = 9.6 Hz, Ar–*H*), 9.24 (1 H, ^3J(H,H) = 10.0 Hz, Ar–*H*), 9.19 (1 H, s, Ar–*H*), 8.92 (1 H, d, ^3J(H,H) = 10.0 Hz, Ar–*H*), 8.86 (1 H, s, Ar–*H*), 4.61 (2H, q, ^3J(H,H) = 7.0 Hz, CH_2), 2.93 (6 H, s, 2 CH_3), 2.86 (6 H, s, 2 CH_3), 1.55 ppm (3H, t, ^3J(H,H) = 7.0 Hz, CH_3). ^{13}C-NMR (125 MHz, methanol-d4, 25 °C): δ = 168.0, 150.2, 134.9, 134.7, 133.3, 132.1, 131.1, 129.4, 127.1, 127.0, 126.9, 126.6, 125.8, 125.5, 124.9, 121.3 (C2), 63.3, 38.4 (C2), 38.0 (C2), 14.9 ppm. MS (ESI): *m*/*z* calc. for $C_{23}H_{25}N_2O_{10}PS_2$: 583.06155 $[M - H]^-$, found: 583.06245.

3,8-Bis(*N*,*N*-dimethylsulfamoyl)-6-(phosphonooxy)pyrene-1-carboxylic acid (3). Compound **1** (4.0 mg, 0.007) was dissolved in an aqueous solution of NaOH (0.05 M, 10 mL). Reaction progress was monitored with RP-TLC and found to be complete after 2 hours. The pH of the reaction solution was neutralized, and water was evaporated from the aqueous phase after extraction with ethyl acetate. The crude product was purified by reverse phase column chromatography (water/methanol = 7 : 3 (v/v)) and yielded **3** as a yellow powder (3.1 mg, 0.006 mmol, 81%). UV/Vis (H_2O): λ_{max} = 407 nm; $\varepsilon_{(407)}$ (H_2O) = 15 000 L mol^{-1} cm^{-1}; fluorescence (H_2O): λ_{max} = 448 nm. ^{1}H-NMR (500 MHz, methanol-d4, 25 °C): δ = 9.25 (1 H, d, ^3J(H,H) = 9.8 Hz, Ar–*H*), 9.24 (1 H, d, ^3J(H,H) = 9.8 Hz, Ar–*H*), 8.97 (1 H, ^3J(H,H) = 10.0 Hz, Ar–*H*), 8.89 (1 H, s, Ar–*H*), 8.87 (1 H, s, Ar–*H*), 8.86 (1 H, d, ^3J(H,H) = 10.0 Hz, Ar–*H*), 2.90 (6 H, s, 2 CH_3), 2.86 ppm (6 H, s, 2 CH_3). ^{13}C-NMR (125 MHz, methanol-d4, 25 °C): δ = 175.5, 149.7, 136.9, 133.1, 132.4, 130.9, 130.7, 129.8, 127.6, 127.5, 127.1, 127.0, 126.8, 126.7, 125.4, 125.3, 121.1, 38.4 (C2), 38.1 (C2) ppm. MS (ESI): *m*/*z* calc. for $C_{21}H_{21}N_2O_{10}PS_2$: 555.03025 $[M - H]^-$, found: 555.03196.

Acknowledgements

Financial support by the German Science Foundation (DFG, JU650/7-1) is gratefully acknowledged. Furthermore we thank Tobias Dier for recording the mass spectra, Volker Huch for X-ray crystallography measurements and Alexander Schiller for the helpful discussion of our manuscript.

Notes and references

1 A. Baruch, D. A. Jeffery and M. Bogyo, Enzyme activity – it's all about image, *Trends Cell Biol.*, 2004, **14**, 29–35.
2 K. Kikuchi, Design, synthesis and biological application of chemical probes for bio-imaging, *Chem. Soc. Rev.*, 2010, **39**, 2048–2053.
3 M. H. Lee, J. S. Kim and J. L. Sessler, Small molecule-based ratiometric fluorescence probes for cations, anions, and biomolecules, *Chem. Soc. Rev.*, 2015, **44**, 4185–4191.
4 J. R. Lakowicz, *Principles of Fluorescence Spectroscopy*, Springer, 3rd edn, 2006.
5 I. Johnson and M. T. Z. Spence, *The Molecular Probes Handbook*, 2010.
6 X. Li, X. Gao, W. Shi and H. Ma, Design strategies for water-soluble small molecular chromogenic and fluorogenic probes, *Chem. Rev.*, 2014, **114**, 590–659.
7 D. J. Yee, V. Balsanek, D. R. Bauman, T. M. Penning and D. Sames, Fluorogenic metabolic probes for direct activity readout of redox enzymes: Selective measurement of human AKR1C2 in living cells, *Proc. Natl. Acad. Sci. U. S. A.*, 2006, **103**, 13304–13309.
8 H. Shi, R. T. K. Kwok, J. Liu, B. Xing, B. Z. Tang and B. Liu, Real-time monitoring of cell apoptosis and drug screening using fluorescent light-up probe with aggregation-induced emission characteristics, *J. Am. Chem. Soc.*, 2012, **134**, 17972–17981.
9 M. Kamiya, D. Asanuma, E. Kuranaga, A. Takeishi, M. Sakabe, M. Miura, T. Nagano and Y. Urano, β-galactosidase fluorescence probe with improved cellular accumulation based on a spirocyclized rhodol scaffold, *J. Am. Chem. Soc.*, 2011, **133**, 12960–12963.

10 A. P. Demchenko, Practical aspects of wavelength ratiometry in the studies of intermolecular interactions, *J. Mol. Struct.*, 2014, **1077**, 51–67.
11 A. P. Demchenko, The concept of λ-ratiometry in fluorescence sensing and imaging, *J. Fluoresc.*, 2010, **20**, 1099–1128.
12 Z.-M. Liu, L. Feng, G.-B. Ge, X. Lv, J. Hou, Y.-F. Cao, J.-N. Cui and L. Yang, A highly selective ratiometric fluorescent probe for in vitro monitoring and cellular imaging of human carboxylesterase 1, *Biosens. Bioelectron.*, 2014, **57**, 30–35.
13 Z. Song, R. T. K. Kwok, E. Zhao, Z. He, Y. Hong, J. W. Y. Lam, B. Liu and B. Z. Tang, A ratiometric fluorescent probe based on ESIPT and AIE processes for alkaline phosphatase activity assay and visualization in living cells, *ACS Appl. Mater. Interfaces*, 2014, **6**, 17245–17254.
14 Y. Kurishita, T. Kohira, A. Ojida and I. Hamachi, Rational design of FRET-based ratiometric chemosensors for in vitro and in cell fluorescence analyses of nucleoside polyphosphates, *J. Am. Chem. Soc.*, 2010, **132**, 13290–13299.
15 L. Chen, *et al.*, The first ratiometric fluorescent probes for aminopeptidase N cell imaging, *Org. Biomol. Chem.*, 2013, **11**, 378–382.
16 T. Komatsu, Y. Urano, Y. Fujikawa, T. Kobayashi, H. Kojima, T. Terai, K. Hanaoka and T. Nagano, Development of 2,6-carboxy-substituted boron dipyrromethene (BODIPY) as a novel scaffold of ratiometric fluorescent probes for live cell imaging, *Chem. Commun.*, 2009, 7015–7017.
17 S. Debieu and A. Romieu, Dual enzyme-responsive 'turn-on' fluorescence sensing systems based on in situ formation of 7-hydroxy-2-iminocoumarin scaffolds, *Org. Biomol. Chem.*, 2015, **13**, 10348–10361.
18 J. Halámek, *et al.*, Multiplexing of injury codes for the parallel operation of enzyme logic gates, *Analyst*, 2010, **135**, 2249–2259.
19 L. Halámková, J. Halámek, V. Bocharova, S. Wolf, K. E. Mulier, G. Beilman, J. Wang and E. Katz, Analysis of biomarkers characteristic of porcine liver injury–from biomolecular logic gates to an animal model, *Analyst*, 2012, **137**, 1768–1770.
20 A. Romieu, 'AND' luminescent 'reactive' molecular logic gates: a gateway to multi-analyte bioimaging and biosensing, *Org. Biomol. Chem.*, 2015, **13**, 1294–1306.
21 Y. Li, H. Wang, J. Li, J. Zheng, X. Xu and R. Yang, Simultaneous intracellular β-D-glucosidase and phosphodiesterase I activities measurements based on a triple-signaling fluorescent probe, *Anal. Chem.*, 2011, **83**, 1268–1274.
22 M. Prost and J. Hasserodt, 'Double gating' - a concept for enzyme-responsive imaging probes aiming at high tissue specificity, *Chem. Commun.*, 2014, **50**, 14896–14899.
23 S.-Y. Li, L.-H. Liu, H. Cheng, B. Li, W.-X. Qiu and X.-Z. Zhang, A dual-FRET-based fluorescence probe for the sequential detection of MMP-2 and caspase-3, *Chem. Commun.*, 2015, **51**, 14520–14523.
24 T.-I. Kim, H. Kim, Y. Choi and Y. Kim, A fluorescent turn-on probe for the detection of alkaline phosphatase activity in living cells, *Chem. Commun.*, 2011, **47**, 9825–9827.
25 J. L. Millán and W. H. Fishman, Biology of human alkaline phosphatases with special reference to cancer, *Crit. Rev. Clin. Lab. Sci.*, 1995, **32**, 1–39.
26 Y. Zhang, W. Chen, D. Feng, W. Shi, X. Li and H. Ma, A spectroscopic off-on probe for simple and sensitive detection of carboxylesterase activity and its application to cell imaging, *Analyst*, 2012, **137**, 716–721.
27 J. Andréasson and U. Pischel, Molecules with a sense of logic: a progress report, *Chem. Soc. Rev.*, 2015, 1053–1069.
28 A. P. de Silva, *Molecular logic-based computation*, RSC Publishing, 2013.
29 K. Szaciłowski, *Infochemistry: Information Processing at the Nanoscale*, Wiley-VCH, 2012.
30 P. Gassman and W. Schenk, A general procedure for the base-promoted hydrolysis of hindered esters at ambient temperatures, *J. Org. Chem.*, 1977, **42**, 918–920.
31 T. Förster, Elektrolytische Dissoziation angeregter Moleküle, *Z. Elektrochem.*, 1950, **54**, 42–46.
32 E. Pines, *The Chemistry of Phenols*, John Wiley & Sons Ltd, 2003.
33 N. Agmon, Elementary steps in excited-state proton transfer, *J. Phys. Chem. A*, 2005, **109**, 13–35.
34 L. M. Tolbert and J. E. Haubrich, Enhanced photoacidities of cyanonaphthols, *J. Am. Chem. Soc.*, 1990, **112**, 8163–8165.
35 L. M. Tolbert and J. E. Haubrich, Photoexcited proton transfer from enhanced photoacids, *J. Am. Chem. Soc.*, 1994, **116**, 10593–10600.
36 D. Huppert, L. M. Tolbert and S. Linares-Samaniego, Ultrafast excited-state proton transfer from cyano-substituted 2-naphthols, *J. Phys. Chem. A*, 1997, **101**, 4602–4605.
37 C. Clower, K. M. Solntsev, J. Kowalik, L. M. Tolbert and D. Huppert, Photochemistry of ' super ' photoacids. 3. excited-state proton transfer from perfluoroalkylsulfonyl-substituted 2-naphthols, *J. Phys. Chem. A*, 2002, **106**, 3114–3122.
38 T.-H. Tran-Thi, C. Prayer, P. Millié, P. Uznanski and J. T. Hynes, Substituent and solvent effects on the nature of the transitions of pyrenol and pyranine. identification of an intermediate in the excited-state proton-transfer reaction, *J. Phys. Chem. A*, 2002, **106**, 2244–2255.
39 K. M. Solntsev, E. N. Sullivan, L. M. Tolbert, S. Ashkenazi, P. Leiderman and D. Huppert, Excited-state proton transfer reactions of 10-hydroxycamptothecin, *J. Am. Chem. Soc.*, 2004, **126**, 12701–12708.
40 M. Prémont-Schwarz, T. Barak, D. Pines, E. T. J. Nibbering and E. Pines, Ultrafast excited state proton transfer reaction of 1-naphthol-3,6-disulfonate and several 5-substituted 1-naphthol derivatives, *J. Phys. Chem. B*, 2013, **117**, 4593–4594.
41 C. Spies, B. Finkler, N. Acar and G. Jung, Solvatochromism of pyranine-derived photoacids, *Phys. Chem. Chem. Phys.*, 2013, **15**, 19893–19905.
42 C. Spies, S. Shomer, B. Finkler, D. Pines, E. Pines, G. Jung and D. Huppert, Solvent dependence of excited-state

proton transfer from pyranine-derived photoacids, *Phys. Chem. Chem. Phys.*, 2014, **16**, 9104–9114.
43 B. Finkler, *et al.* Highly photostable 'super'-photoacids for ultrasensitive fluorescence spectroscopy, *Photochem. Photobiol. Sci.*, 2014, **13**, 548–562.
44 C. Hansch, A. Leo and R. W. Taft, A survey of Hammett substituent constants and resonance and field parameters, *Chem. Rev.*, 1991, **91**, 165–195.
45 H. N. Fernley and P. G. Walker, Kinetic behaviour of calf-intestinal alkaline phosphatase with 4-methylumbelliferyl phosphate, *Biochem. J.*, 1965, **97**, 95–103.
46 S. Lun and W. R. Bishai, Characterization of a novel cell wall-anchored protein with carboxylesterase activity required for virulence in mycobacterium tuberculosis, *J. Biol. Chem.*, 2007, **282**, 18348–18356.
47 L. Provencher and J. B. Jones, A concluding specification of the dimensions of the active site model of pig liver esterase, *J. Org. Chem.*, 1994, **59**, 2729–2732.
48 P. D. De María, C. A. García-Burgos, G. Bargeman and R. W. Van Gemert, Pig liver esterase (PLE) as biocatalyst in organic synthesis: From nature to cloning and to practical applications, *Synthesis*, 2007, **10**, 1439–1452.
49 J. L. Ward and C. M. Tse, Nucleoside transport in human colonic epithelial cell lines: evidence for two Na+-independent transport systems in T84 and Caco-2 cells, *Biochim. Biophys. Acta, Biomembr.*, 1999, **1419**, 15–22.
50 M. Pastor-Anglada, P. Cano-Soldado, M. Molina-Arcas, M. P. Lostao, I. Larráyoz, J. Martínez-Picado and F. J. Casado, Cell entry and export of nucleoside analogues, *Virus Res.*, 2005, **107**, 151–164.
51 M. N. Win and C. D. Smolke, Higher-order cellular information processing with synthetic RNA devices, *Science*, 2008, **322**, 456–460.
52 M. Elstner, J. Axthelm and A. Schiller, Sugar-based molecular computing by material implication, *Angew. Chem., Int. Ed.*, 2014, **53**, 7339–7343.
53 J. Ditkovich, T. Mukra, D. Pines, D. Huppert and E. Pines, Bifunctional photoacids: Remote protonation affecting chemical reactivity, *J. Phys. Chem. B*, 2015, **119**, 2690–2701.
54 B. Zelent, J. M. Vanderkooi, R. G. Coleman, I. Gryczynski and Z. Gryczynski, Protonation of excited state pyrene-1-carboxylate by phosphate and organic acids in aqueous solution studied by fluorescence spectroscopy, *Biophys. J.*, 2006, **91**, 3864–3871.
55 N. V. Nucci, B. Zelent and J. M. Vanderkooi, Pyrene-1-carboxylate in water and glycerol solutions: Origin of the change of pK upon excitation, *J. Fluoresc.*, 2008, **18**, 41–49.
56 B. Zelent, J. M. Vanderkooi, N. V. Nucci, I. Gryczynski and Z. Gryczynski, Phosphate assisted proton transfer in water and sugar glasses: A study using fluorescence of pyrene-1-carboxylate and IR spectroscopy, *J. Fluoresc.*, 2009, **19**, 21–31.
57 A. Weller, Outer and inner mechanism of reactions of excited molecules, *Discuss. Faraday Soc.*, 1959, **27**, 28–33.
58 A. Weller, Fast reactions of excited molecules, *Prog. React. Kinet.*, 1961, **1**, 187–214.
59 D. B. Spry and M. D. Fayer, Observation of slow charge redistribution preceding excited-state proton transfer, *J. Chem. Phys.*, 2007, **127**, 204501.
60 E. Pines, D. Pines, Y.-Z. Ma and G. R. Fleming, Femtosecond pump–probe measurements of solvation by hydrogen-bonding interactions, *ChemPhysChem*, 2004, **5**, 1315–1327.
61 D. B. Spry and M. D. Fayer, Observation of slow charge redistribution preceding excited-state proton transfer, *J. Chem. Phys.*, 2007, **127**, 204501.
62 C. Spies, B. Finkler, N. Acar and G. Jung, Solvatochromism of pyranine-derived photoacids, *Phys. Chem. Chem. Phys.*, 2013, **15**, 19893–19905.
63 H. Offenbacher, O. S. Wolfbeis and E. Furlinger, Fluorescence optical sensors for continuous determination of near-neutral pH values, *Sens. Actuators*, 1986, **9**, 73–84.
64 G. M. Ullmann, Relations between protonation constants and titration curves in polyprotic acids: A critical view, *J. Phys. Chem. B*, 2003, **107**, 1263–1271.
65 R. Bizzarri, *et al.* Green fluorescent protein ground states: The influence of a second protonation site near the chromophore, *Biochemistry*, 2007, **46**, 5494–5504.
66 A. P. de Silva, N. H. Q. Gunaratne and C. P. McCoy, A molecular photoionic AND gate based on fluorescent signalling, *Nature*, 1993, **364**, 42–44.
67 J. Andréasson and U. Pischel, Smart molecules at work-mimicking advanced logic operations, *Chem. Soc. Rev.*, 2010, **39**, 174–188.
68 A. P. de Silva and N. D. McClenaghan, Molecular-scale logic gates, *Chem. – Eur. J.*, 2004, **10**, 574–586.
69 A. Coskun, E. Deniz and E. U. Akkaya, Effective PET and ICT switching of boradiazaindacene emission: A unimolecular, emission-mode, molecular half-subtractor with reconfigurable logic gates, *Org. Lett.*, 2005, **7**, 5187–5189.
70 J. Andréasson, U. Pischel, S. D. Straight, T. a. Moore, A. L. Moore and D. Gust, All-photonic multifunctional molecular logic device, *J. Am. Chem. Soc.*, 2011, **133**, 11641–11648.
71 J. Andréasson, S. D. Straight, T. A. Moore, A. L. Moore and D. Gust, Molecular all-photonic encoder-decoder, *J. Am. Chem. Soc.*, 2008, **130**, 11122–11128.
72 D. Kang, R. J. White, F. Xia, X. Zuo, A. Vallée-Bélisle and K. W. Plaxco, DNA biomolecular-electronic encoder and decoder devices constructed by multiplex biosensors, *NPG Asia Mater.*, 2012, **4**, e1.
73 R. Orbach, F. Remacle, R. D. Levine and I. Willner, DNAzyme-based 2:1 and 4:1 multiplexers and 1:2 demultiplexer, *Chem. Sci.*, 2014, **5**, 1074–1081.
74 L. Zhao, W. Xia and C. Yang, Fluorescent 1:2 demultiplexer and half-subtractor based on the hydrolysis of N-salicylidene-3-aminopyridine, *Spectrochim. Acta, Part A*, 2014, **117**, 397–401.
75 J. Andréasson, G. Kodis, Y. Terazono, P. A. Liddell, S. Bandyopadhyay, R. H. Mitchell, T. A. Moore, A. L. Moore

and D. Gust, Molecule-based photonically switched half-adder, *J. Am. Chem. Soc.*, 2004, **126**, 15926–15927.

76 F. Remacle, R. Weinkauf and R. D. Levine, Molecule-based photonically switched half and full adder, *J. Phys. Chem. A*, 2006, **110**, 177–184.

77 H. Pei, L. Liang, G. Yao, J. Li, Q. Huang and C. Fan, Reconfigurable three-dimensional DNA nanostructures for the construction of intracellular logic sensors, *Angew. Chem., Int. Ed.*, 2012, **51**, 9020–9024.

78 D. Margulies, G. Melman and A. Shanzer, Fluorescein as a model molecular calculator with reset capability, *Nat. Mater.*, 2005, **4**, 768–771.

79 D. Margulies, G. Melman and A. Shanzer, A molecular full-adder and full-subtractor, an additional step toward a moleculator, *J. Am. Chem. Soc.*, 2006, **128**, 4865–4871.

80 D. Margulies, C. E. Felder, G. Melman and A. Shanzer, A molecular keypad lock: A photochemical device capable of authorizing password entries, *J. Am. Chem. Soc.*, 2007, **129**, 347–354.

81 P. Remón, M. Hammarson, S. Li, A. Kahnt, U. Pischel and J. Andréasson, Molecular implementation of sequential and reversible logic through photochromic energy transfer switching, *Chem. – Eur. J.*, 2011, **17**, 6492–6500.

82 Q. Li, Y. Yue, Y. Guo and S. Shao, Fluoride anions triggered 'OFF–ON' fluorescent sensor for hydrogen sulfate anions based on a BODIPY scaffold that works as a molecular keypad lock, *Sens. Actuators, B*, 2012, **173**, 797–801.

83 X.-J. Jiang and D. K. P. Ng, Sequential logic operations with a molecular keypad lock with four inputs and dual fluorescence outputs, *Angew. Chem., Int. Ed.*, 2014, **53**, 10481–10484.

84 B. Rout, P. Milko, M. A. Iron, L. Motiei and D. Margulies, Authorizing multiple chemical passwords by a combinatorial molecular keypad lock, *J. Am. Chem. Soc.*, 2013, **135**, 15330–15333.

85 G. Strack, M. Ornatska, M. Pita and E. Katz, Biocomputing security system: concatenated enzyme-based logic gates operating as a biomolecular keypad lock, *J. Am. Chem. Soc.*, 2008, **130**, 4234–5235.

86 J. Chen, S. Zhou and J. Wen, Concatenated logic circuits based on a three-way DNA junction: A keypad-lock security system with visible readout and an automatic reset function, *Angew. Chem., Int. Ed.*, 2014, **54**, 446–450.

87 A. P. de Silva and N. D. McClenaghan, Proof-of-principle of molecular-scale arithmetic, *J. Am. Chem. Soc.*, 2000, **122**, 3965–3966.

88 P. Remón, M. Bälter, S. Li, J. Andréasson and U. Pischel, An all-photonic molecule-based D flip-flop, *J. Am. Chem. Soc.*, 2011, **133**, 20742–20745.

89 Y. Liu, W. Jiang, H. Y. Zhang and C. J. Li, A multifunctional arithmetical processor model integrated inside a single molecule, *J. Phys. Chem. B*, 2006, **110**, 14231–14235.

90 R. Gotor, A. M. Costero, S. Gil, M. Parra, P. Gaviña and K. Rurack, Boolean operations mediated by an ion-pair receptor of a multi-readout molecular logic gate, *Chem. Commun.*, 2013, **49**, 11056–11058.

91 M. Vester, T. Staut, J. Enderlein and G. Jung, Photon antibunching in a cyclic chemical reaction scheme, *J. Phys. Chem. Lett.*, 2015, **6**, 1149–1154.

92 M. Vester, A. Grueter, B. Finkler, R. Becker and G. Jung, Biexponential photon antibunching: Recombination kinetics within the Forster-cycle in DMSO, *Phys. Chem. Chem. Phys.*, 2016, **18**, 10281–10288.

93 R. K. Sehgal and S. Kumar, A simple preparation of 1-hydroxypyrene, *Org. Prep. Proced. Int. New J. Org. Synth.*, 1989, **21**, 223–225.